DENTAL MATERIALS 26 (2010) 589–599

available at www.sciencedirect.com

ScienceDirect

journal homepage: www.intl.elsevierhealth.com/journals/dema

Material properties and fractography of an indirect dental resin composite

*Janet B. Quinn, George D. Quinn**

ADAF Paffenbarger Research Center, NIST, Gaithersburg, MD, USA

ARTICLE INFO

Article history:
Received 3 September 2009
Received in revised form
2 December 2009
Accepted 23 February 2010

Keywords:
Composite
Resin
Material properties
Strength
Hardness
Indentation size effect
Fractography
Fracture mirror
Fracture origin
Failure analysis
R-Curve

ABSTRACT

Objectives. Determination of material and fractographic properties of a dental indirect resin composite material.

Methods. A resin composite (Paradigm, 3M-ESPE, MN) was characterized by strength, static elastic modulus, Knoop hardness, fracture toughness and edge toughness. Fractographic analyses of the broken bar surfaces was accomplished with a combination of optical and SEM techniques, and included determination of the type and size of the failure origins, and fracture mirror and branching constants.

Results. The flexure test mean strength ± standard deviation was 145 ± 17 MPa, and edge toughness, T_e, was 172 ± 12 N/mm. Knoop hardness was load dependent, with a plateau at 0.99 ± 0.02 GPa. Mirrors in the bar specimens were measured with difficulty, resulting in a mirror constant of approximately 2.6 MPa $m^{1/2}$. Fracture in the bar specimens initiated at equiaxed material flaws that had different filler concentrations that sometimes were accompanied by partial microcracks. Using the measured flaw sizes, which ranged from 35 to 100 μm in size, and using estimates of the stress intensity shape factors, fracture toughness was estimated to be 1.1 ± 0.2 MPa $m^{1/2}$.

Significance. Coupling the flexure tests with fractographic examination enabled identification of the intrinsic strength limiting flaws. The same techniques could be useful in determining if clinical restorations of similar materials fail from the same causes. The existence of a strong load-dependence of the Knoop hardness of the resin composite is not generally mentioned in the literature, and is important for material comparisons and wear evaluation studies. Finally, the edge toughness test was found promising as a quantitative measure of resistance to edge chipping, an important failure mode in this class of materials.

1. Introduction

Resin composites are becoming increasingly important in dentistry, with expanding application resulting from processing and material innovations [1,2]. Many of the improvements in this class of materials, particularly those stemming from filler particle type and loading increases, are based on material property measurements. Among the published dental composite strength values, however, there is little associated fractographic analysis. This is important, as measured material strength alone is not necessarily indicative of the causes of restoration failure or clinical longevity [3].

* *Corresponding author at*: ADAF Paffenbarger Research Center, Mailstop 8546, National Institute of Standards and Technology, Gaithersburg, MD 20878, USA. Tel.: +1 301 975 5765; fax: +1 301 963 9143.
E-mail address: george.quinn@nist.gov (G.D. Quinn).

0109-5641/$ – see front matter © 2010 Academy of Dental Materials. Published by Elsevier Ltd. All rights reserved.
doi:10.1016/j.dental.2010.02.008

For brittle materials outside the dental field, systematic correlations of strength test values and component performance commonly use fractographic analyses [4]. A study of commercial glass-ceramics, a class of materials widely used in dentistry, determined that different batches had identical elastic moduli, fracture toughnesses, densities and microstructures, but very different failure loads due to a variation in flaw type [5]. Similar examples can be found for alumina-based ceramics [6,7]. Fractographic examination is essential for critical flaw determination and component strength predictions for brittle materials.

Among brittle materials, highly filled resin composites are somewhat neglected in fractographic analyses [8]. This class of materials falls "in between" polymers and ceramics. Fractographic specialists in either field find features difficult to discern when they are masked by rough microstructures that are often typical in failed composite components [9]. An important but overlooked resource is a 1989 book on fractography of polymers and composites by Roulin-Moloney [10] which includes a chapter on unfilled and filled epoxy resins.

In this study, mechanical property testing and fractographic analysis was applied to a commercial dental composite. The well-characterized stress configuration of a simple bend bar can be very helpful in relating fractographic markings to behavior, especially in an unfamiliar "fractographically difficult" material. The translucency of the material evaluated in the present study initially made examination difficult, but with proper illumination, the relevant features became easy to detect and interpret. Once the correct fracture origin areas were identified by optical microcopy, then scanning electron microscopy was used to characterize the fracture origins. The very fine size of the filler particles also helped since the fracture surface was not too rough. Coarse- or medium-sized fillers lead to very rough fracture surfaces that can mask critical fractographic markings. Property tests also included edge chipping characterization, an important failure mechanism for composite dental restorations [11]. The emphasis of the resin composite property tests and fractography of this study is on practical analyses that could be relevant to failure investigations of resin composite restorations. Our null hypothesis is that fractographic analysis can be used to identify key features associated with the mechanical properties.

2. Materials and methods

2.1. Material

Dental resin composite mill blocks (Paradigm, 3 M ESPE, St. Paul, MN)[1] were donated by the manufacturer for the property tests. The company literature [e.g., [12,13]] lists the material as containing 0.85 mass fraction spherical sol gel derived particles comprising nanocrystalline zirconia in silica. The spherical particles averaged 0.6 μm in size, but had a broad size distribution, within a highly cross-linked polymeric matrix of bis-GMA and TEGDMA. A silane aided bonding to the filler. The flexural strength, σ_f, is reported to be 145 ± 15 MPa; fracture toughness, K_{Ic} is 1.3 ± 0.1 MPa $m^{1/2}$; and a Young's modulus in compression of about 7 GPa and a flexural modulus of about 12 GPa. The company literature does not include a statement of uncertainty with the material description.

2.2. Strength

Bars ($n = 18$) were professionally machined (BOMAS, Somerville, MA) and finished according to the recommendations in ASTM C1161 [14], which is intended for use with brittle ceramics, but is also useful for brittle filled composites. Because of limitations in the length of the original resin composite cylinder blanks, the final bar sizes of 3 mm × 4 mm × 18 mm were much shorter than the > 40 mm specimen size B specimen lengths in the referenced standard. Small bevels were applied to all four long edges to eliminate any edge damage. Short, stubby bend bars should not be tested in 4-point bending because excessive errors can result [15], (e.g., from tiny fixture misalignments or wedging stresses at the contact points) so in this instance 3-point was preferred, albeit at the cost of exposing only a tiny portion of the bar to the full tensile stresses. The bars were broken on an Instron Universal Testing Machine (Model 1122, Canton, MA) in 3-point flexure with a crosshead speed of 0.5 mm/min. The semi-articulating, self-aligning fixture had a 16 mm outside roller span and the rollers were free to roll to eliminate friction errors. The fracture stress, σ_f, was calculated by the formula:

$$\sigma_f = \frac{3PL}{2}(\text{width} \times \text{height}^2) \quad (1)$$

where P is the break load and L is the 16 mm span. The specimen widths and heights were measured with a micrometer with a resolution of 0.001 mm. The Weibull parameters were estimated by maximum likelihood estimation (MLE)[2] in accordance with ASTM C 1239 [16].

2.3. Elastic modulus

This property was evaluated by measuring the deflection of the flexural strength bars. The machine compliance was obtained by inserting a large alumina block in the fixtures and repeatedly loading to 100 N. The resulting displacement measurement was assumed to be due entirely to the machine, load cell and fixtures, and was subtracted from the displacement measured in the flexural tests for the same load increment, ΔP, to obtain the displacement solely due to specimen flexure. The static elastic modulus, E, of the resin composite could then be

[1] Commercial products and equipment are identified only to specify adequately experimental procedures and does not imply endorsement by the authors, institutions or organizations supporting this work, nor does it imply that they are necessarily the best for the purpose.

[2] MLE analysis is favored by many and used in many international standards since the confidence band intervals on Weibull parameter estimates are tighter than those from linear regression analysis.

calculated by:

$$E = \frac{\Delta P \times L^3}{4}(\text{width} \times \text{height}^3 \times \text{specimen displacement}) \quad (2)$$

where ΔP is the load differential for a finite specimen displacement taken at midspan.

2.4. Hardness

Knoop hardness values (HK) were obtained using a Wilson/Instron Tukon Model 300 Hardness Machine (Canton, MA). Hardness values of brittle materials generally increase as indentation forces decrease, a phenomenon known as the indentation size effect (ISE) [17]. Because of the ISE, a specified force or functional relationship over a test range is necessary to accurately compare the hardness of brittle dental materials. Hardness measurements were made at forces ranging from 0.25 to 9.8 N, with ten indentations at each force. The hardness at the three highest forces (4.9, 6.9 and 9.8 N) showed no significant difference using Tukey's multiple pairwise comparison at 99% family confidence level. The combined data from these three loads constitute the reported load-independent hardness. The hardness readings were made in air under room conditions, but ten indentations at 9.8 N were also made on a specimen surface wet with distilled water to determine whether the surface environment and short time exposure to water had any influence on hardness.

2.5. Edge toughness

Edge toughness (also known as edge strength or edge flaking resistance) measures the susceptibility of a material to edge chipping [18–25]. In this test, an increasing force is applied near the edge of a specimen until a chip is formed. At greater distances from the specimen edge, higher forces are required for chip formation. A plot can be constructed by plotting the force necessary to form a chip against the distance from the specimen edge. The slope of a straight line resulting from such a plot constitutes the edge toughness, T_e, although a power law often better fits the edge toughness plot for glasses and porcelains [23,24]. High values of T_e, or steep plots, indicate a material is highly resistant to edge chipping. Low T_e values indicate that large chips form at low loads, and the material chips easily. Other indenter shapes are now in use, but we prefer to use a sharp conical indenter since they are inexpensive, easy to replace, and the indentation shape is self similar as indentation load is increased. An Engineering Systems Model CK 10 edge-chip machine (Nottingham, UK), fitted with a conical 120° diamond scribe indenter, was used to form chips and measure forces in this study. The tip was sharp, with a radius of less than 10 μm. More detailed descriptions and photographs of the equipment that was used in the edge chipping test are included in Ref. [25].

2.6. Fractography

Fractographic examination and measurements were made with a scanning electron microscope (SEM) (JEOL 5300, Peabody, MA) at up to 1500× and a stereoptical microscope (Leica MZ16, Wetzlar, Germany) at up to 92×. The translucency and internal light scattering hampered conventional reflected light optical observation of fracture surface markings so special illumination procedures were required. For optical examinations of the bar specimen fracture surfaces, *transillumination* was particularly helpful in identifying fracture origins, and oblique lighting on gold-coated surfaces aided fracture mirror boundary delineation. It was critical to have directed illumination from one or two fiber optic light guides (as opposed to a ring light) for these examinations. The optical microscope was equipped with a traveling stage enabling size measurements with a resolution of 1 μm. Additional information about the fractographic techniques and equipment may be found in Ref. [26].

Fracture mirrors were detected and their sizes measured after the specimen surfaces were gold coated to make the fracture surface easier to interpret. Mirror sizes are related to the fracture stress by Orr's equation [26,27]:

$$\sigma_f = A(R)^{-1/2} \quad (3)$$

where R is the mirror radius and A is a materials property known as the mirror constant which has units of MPa $m^{1/2}$. Ref. [26] has detailed tabulations of A values for glasses and ceramics. A similar relationship exists for fracture branching, where the crack first splits into two or more cracks. Branching distances were measured along the tension surface.

2.7. Fracture toughness

Attempts were made to measure fracture toughness by the surface crack in flexure (SCF) method in accordance with ASTM C 1421 [28]. This method has been successfully applied to dental porcelains [29], but was unsuccessful with the composite resin in this study. The SCF method uses a Knoop indentation to create a median crack in a bend bar. The indentation residual stress damage zone is removed by polishing, the bar is broken in four-point bending, the fracture strength computed, the median crack size is measured on the fracture surface, and appropriate formulas for the stress intensity [28] used to compute fracture toughness. Although this dental composite resin is brittle, indentation loads up to 4.9 N did not create large median type cracks beneath the indentation. Large indentations, nearly a millimeter in length, were created but the material was too soft to form subsurface semielliptical cracks. Fracture toughness estimates were instead obtained from the intrinsic flaws in the eighteen flexural strength test specimens. The flaws were modeled by simple elliptical or semi-elliptical cracks located at the specimen surface or in the interior. In the latter case, which occurred for three flexural test specimens, the stresses were corrected for the origin location beneath the surface. Fracture toughness was computed by:

$$K_{Ic} = Y\sigma_f\sqrt{a} \quad (4)$$

where Y is geometric stress intensity shape factor, σ_f is the fracture stress, and a is the flaw size. Y factors were calculated in accordance with the Newman–Raju stress intensity equations in Refs. [28,30,31] for shallow semielliptical surface flaws

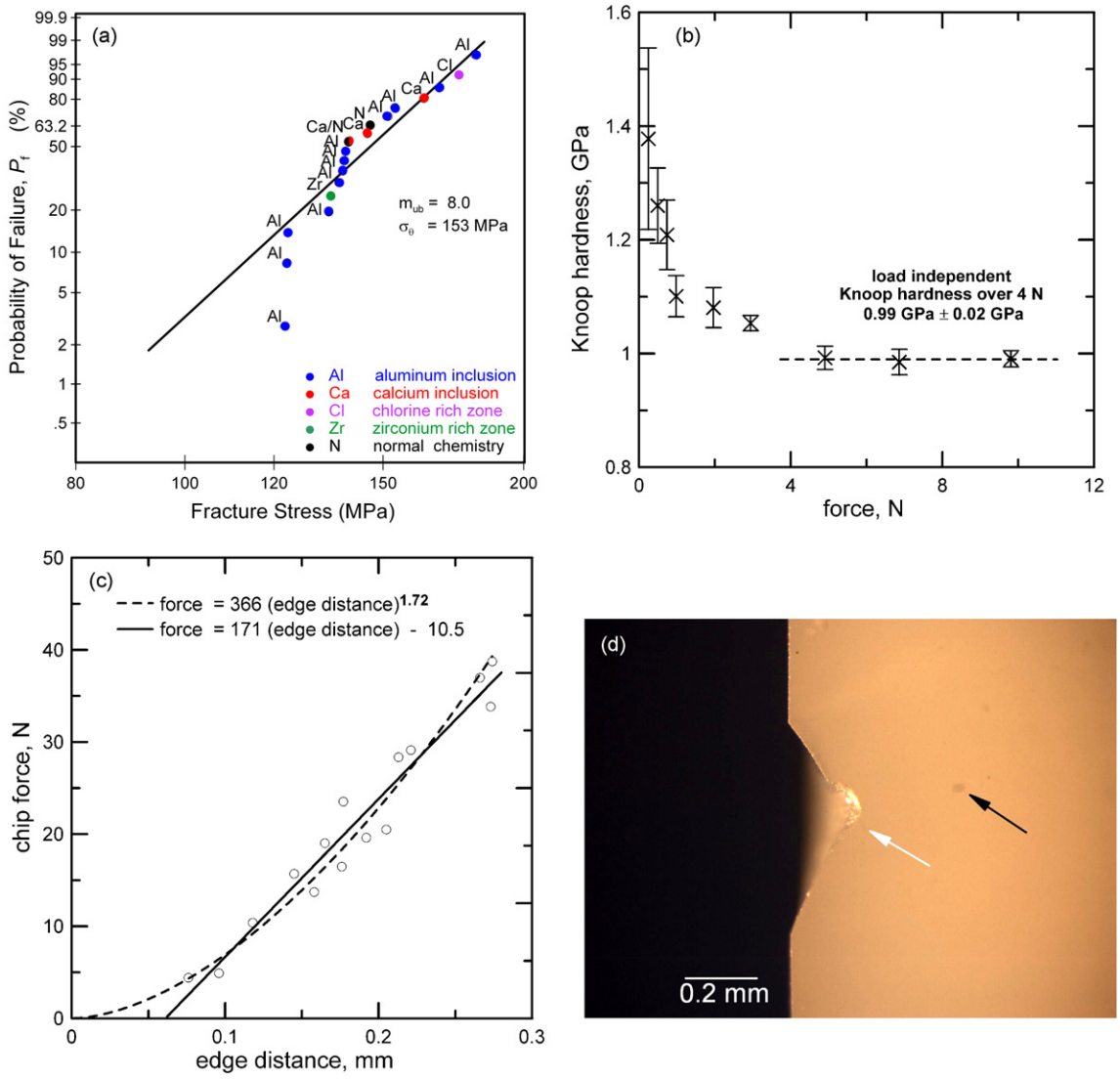

Fig. 1 – Material properties of the resin composite specimens: (a) Weibull graph of composite strengths, (b) Knoop hardness plot illustrating the hardness/load dependence, (c) edge chipping plot and (d) top optical view of an edge chip (white arrow). The small, barely visible darker area (black arrow) is similar to those found at the resin composite fracture origins.

and Refs. [30,31] for deep semielliptical surface flaws or fully elliptical flaws in the interior. The flaw sizes were measured on scanning electron microscope images at 500× to 1500× magnification so that the flaw covered at least half the field of view. Additional measurements were made with the traversing stage and stereoptical microscope at 92× magnification.

3. Results

3.1. *Material properties*

The average fracture strength, σ_f, was 145 MPa and the standard deviation was 17 MPa.[3] The load displacement traces were linear to fracture. Fig. 1a shows a Weibull graph for the 18 data points. The unbiased maximum likelihood estimation (MLE) fit gave a Weibull modulus of 8.0 (90% confidence limits as per [16]: 6.8–12.9) and a characteristic strength of 153 MPa (90% confidence limits: 145–161 MPa). The wiggles in the curve are not unusual for a small sample set of only 18 specimens. The two weakest specimens hint that there may be a threshold strength of the order of 100–120 MPa, but more testing would be necessary to make any definitive conclusions. The static flexural elastic modulus was 12.2 ± 0.8 GPa.

The Knoop hardness exhibited a strong indentation size effect at low loads, as shown in Fig. 1b. There is no significant difference (as defined in Section 2) among the hardness values collected after 4 N, and for loads greater than this, the load-independent Knoop hardness is 0.99 ± 0.02 GPa. The measured Knoop hardness of the specimens indented under distilled water was not significantly different at 0.98 ± 0.01 GPa.

The edge toughness plot for the resin composite comprises Fig. 1c. Two curve fits are shown for comparison: one is a lin-

[3] Unless otherwise stated, all uncertainties are one standard deviation.

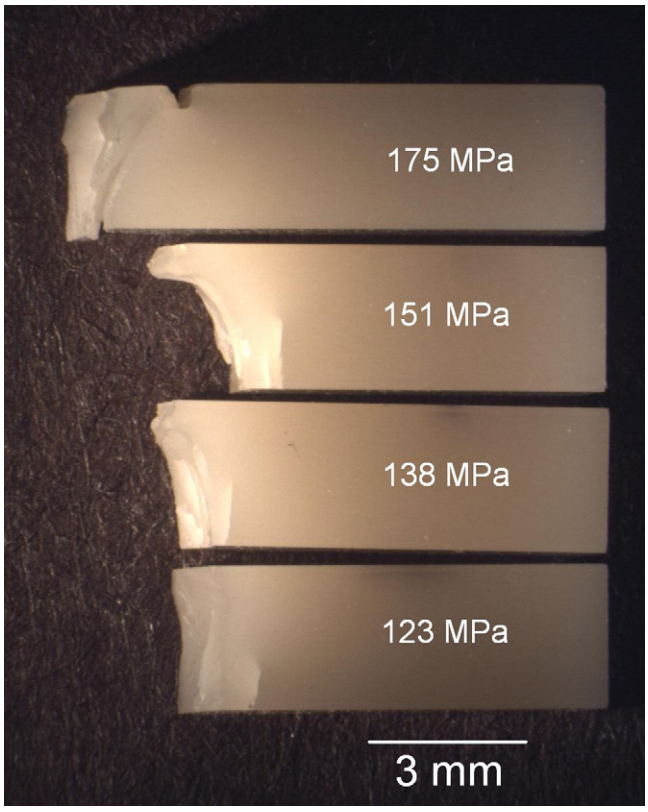

Fig. 2 – Side view of typical broken flexure bars, showing the compression curls. The tensile surface is on the bottom. The white labels indicate the flexure strength of each bar.

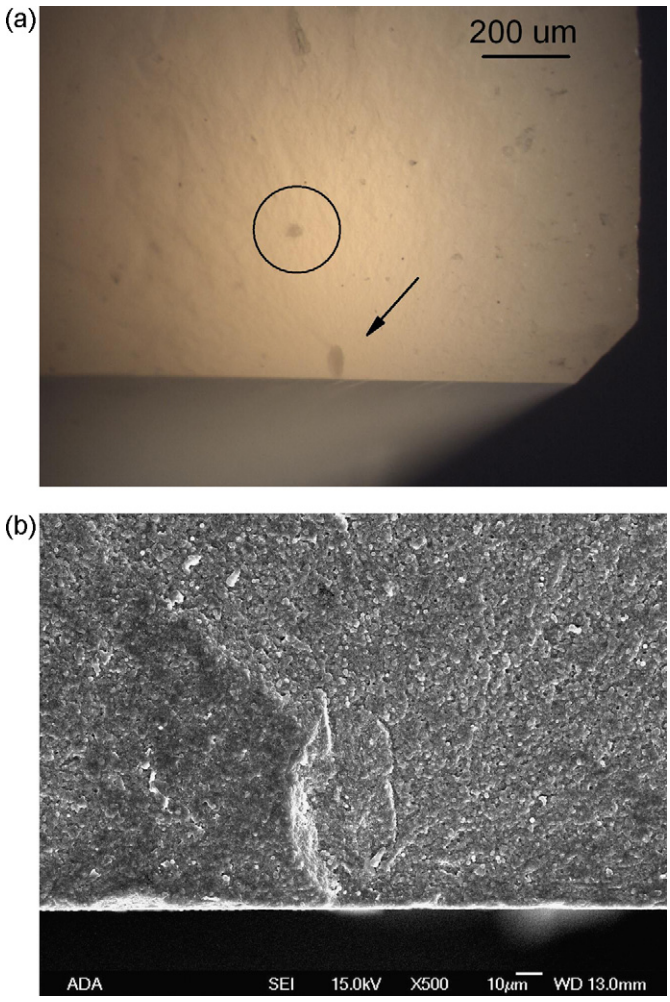

Fig. 3 – A flexure bar fracture surface. (a) Optical transillumination shows the fracture origin from which fracture originated (arrow). A second similar feature is circled, indicating this feature type is volume distributed. (b) The SEM photo of the origin flaw (arrows) shows the aluminum inclusion origin with partial microcracking around its periphery.

ear and the other a power law fit. As in many glass-ceramics, a power law fits the data well [23,24], as shown by the least squares fitted dotted line, with a coefficient of determination, R^2, of 0.95. The power law fit is: chip force (N) = 366 × (edge distance in mm)$^{1.72}$. The plot also shows a solid linear regression fit that does not go through zero. The linear fit has the same R^2 of 0.95 and the relationship is: chip force (N) = 171.5 × (edge distance in mm) – 10.5 mm. The slope of the linear fit is defined as the edge toughness: $T_e = 171.5 \pm 11.5$ N/mm. Fig. 1d is a photomicrograph of a typical edge chip. The black arrow in the photo points to a small dark inhomogeneity within the material. Such inhomogeneites were the strength limiting flaws as discussed in the next section.

3.2. *Fractography*

Many fractographic features similar to those found in failed ceramic components (compression curl, branching, hackle, fracture mirror) were found in the dental composite flexure bars. Fig. 2 shows side views of typical broken specimens. The specimen compression zones at the top of the bars exhibit the compression curl that results from flexure tests of brittle materials [26]. The specimens that broke at higher stresses have rougher surfaces and more crack branching. Higher strength specimens have greater stored elastic energy that can be converted to specimen surface energy, thereby creating more cracks and rougher surfaces.

Fig. 3 shows an optical (a) and a higher magnification SEM (b) micrograph of a specimen fracture surface. In Fig. 3a, transillumination reveals a small dark area at the fracture origin (arrow). This finding was typical of all but three of the fractured specimens and the origin areas were sometimes discernable on only one specimen half. When the light is adjusted at different angles, these small areas can easily be made to appear either lighter or darker than the surrounding material. With patience, other similar small areas could be found away from the origins on or beneath the specimen machined surfaces as well as on fracture surfaces. Examples are circled in the Fig. 3a photo and indicated by the arrow in Fig. 1d. Such discontinuities were sometimes difficult to discern in the SEM and optical photos were essential to facilitate finding the fracture origins in the SEM.

The flaws ranged from elongated spheres to elliptical regions with aspect ratios up to 2:1. The flaw diameters ranged

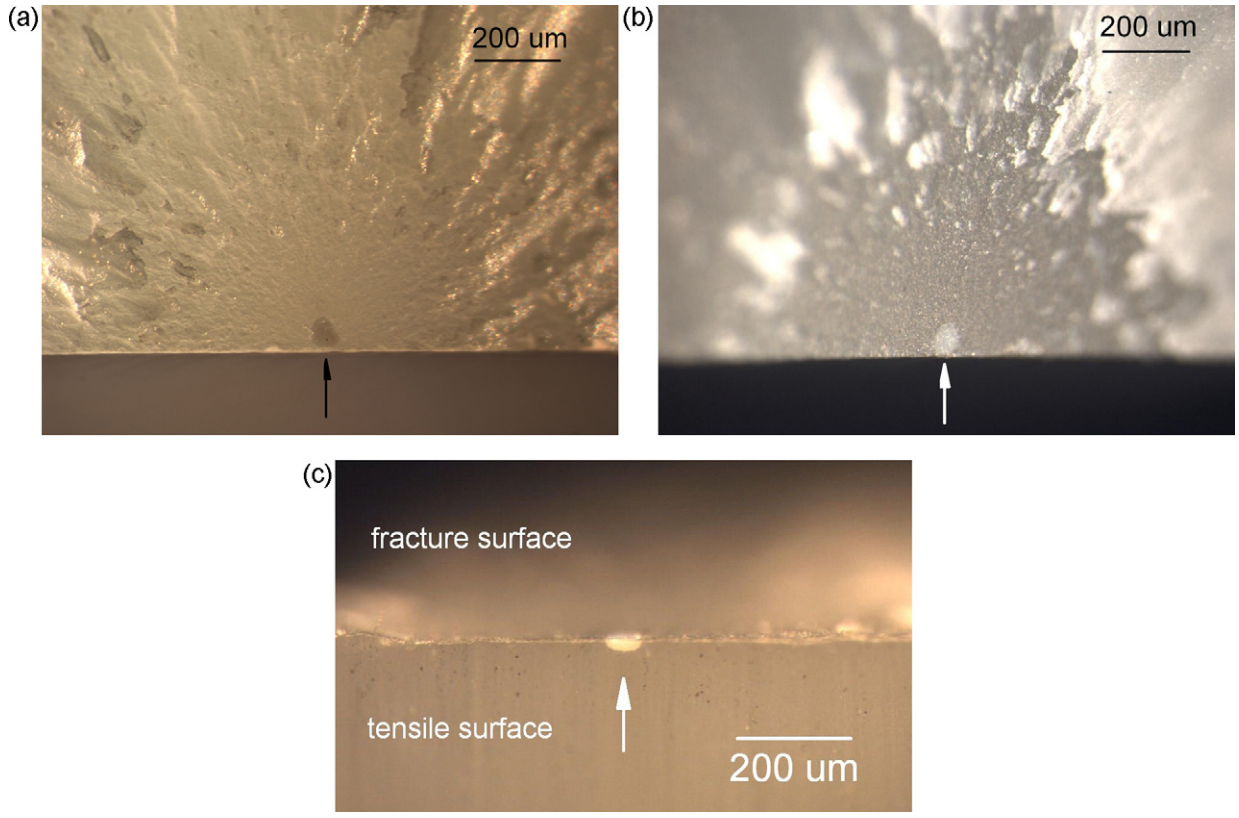

Fig. 4 – Optical images of an origin flaw in a flexure bar (138 MPa). Depending upon the lighting, the aluminum rich inclusion flaw (marked by arrows) may appear as a dark spot (a) or a bright spot (b). (c) shows the bar tilted at an angle.

from as low as 35 μm to as large as 100 μm. Initially it was thought that the flaws were filler agglomerates or regions of nonuniform mixing in the composite, but x-ray energy dispersive analysis in the SEM revealed that 16 of the 18 fracture origins were chemical heterogeneities or inclusions. Many of the origin sites had evidence of debonding around the flaw periphery. The debonding caused light to reflect at the flaw periphery, causing the flaws to stand out quite clearly as dark areas or bright spots if they reflected light back to the viewer. The majority of the flaws, such as those shown in Figs. 3–5, were aluminum rich, but two were calcium rich such as shown in Fig. 6.

Fig. 5a and b shows a fracture origin whereby transillumination was very effective. Hackle lines emanate from a fracture mirror centered on the fracture origin which was a dark spot at the edge chamfer. These first two images are included since, although they not entirely clear due to the internal reflections and translucency, they nonetheless illustrate what type of markings can be detected optically with the right lighting. The SEM images of the mating half in Fig. 5c and d reveal more about the character of the flaw. The backscattered electron mode (Fig. 5c) reveals the very different microstructure of the flaw compared to the surrounding material. The secondary electron image (Fig. 5d) gives better topographical information showing how the flaw has microcracking and partial detachment around its periphery. X-ray energy dispersive analysis revealed this flaw was an aluminum rich inclusion.

Fig. 6 shows an internal fracture origin with an altogether different appearance than the surrounding material. The flaw is a calcium rich inclusion which has very few filler particles within the flaw. There is also some porosity in the flaw.

The flaw sizes and shapes were used to estimate fracture toughness. The origins were often equiaxed in shape, but many had elliptical or semielliptical cross sections. In every case, the flaw width (2c) and depth (a or 2a, depending upon whether the flaw was at the tensile surface or in the interior) was measured and the appropriate dimensions used to compute the Y factors and the fracture toughness in accordance with Eq. (4). The fracture toughness was calculated as $1.1 \pm 0.2\,\mathrm{MPa\,m^{1/2}}$.

3.3. *Fracture mirror and branching constants*

The same specimen surface that is shown in Fig. 3 is shown in the Fig. 7a optical photomicrograph. The specimen is now gold coated and viewed with oblique lighting to better reflect fracture surface features and eliminate light scattering from beneath the fracture surface. The smooth area surrounding the origin is the fracture mirror. Mirrors were visually obvious in all the resin composite specimens of this study, but it was difficult to define the mirror boundaries. The white arrows in Fig. 7a represent subjective judgment of the mirror size, measured by the traveling stage attached to the optical microscope. Fig. 7b is a plot of the strength *vs.* $(\text{mirror radius})^{-1/2}$. The slope is the mirror constant, A_0, where the subscript

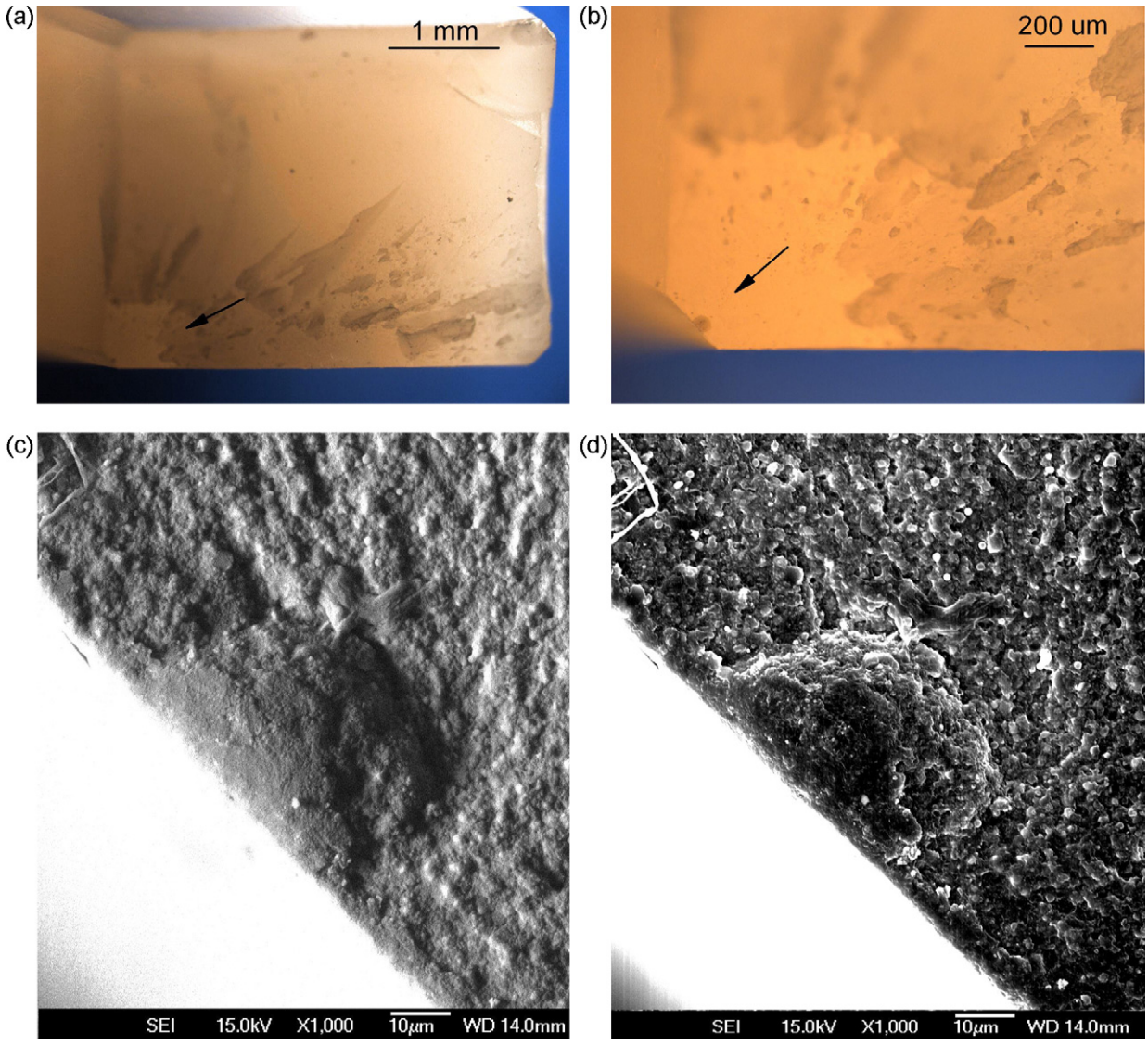

Fig. 5 – Fracture origin in a flexure bar (σ_f = 139 MPa). (a) and (b) are optical images using transillumination. The origin is the dark round spot at the chamfer marked by the arrows. (c) and (d) are backscattered and secondary electron mode SEM close ups of the aluminum inclusion flaw, respectively.

denotes "outer" or the mirror-hackle boundary [26]. The slope is force-fit through the origin, with a correlation coefficient R^2 of 0.998. From the graph, an approximate mirror constant of $2.6 \pm 0.1\,\text{MPa}\,\text{m}^{1/2}$ is obtained. A similar analysis for the crack branching distance (where a crack first split into two or more propagating cracks) gave an estimate of the branching constant, A_b, of $2.9 \pm 0.1\,\text{MPa}\,\text{m}^{1/2}$.

4. Discussion

Not surprisingly, the mechanical properties were generally similar to those reported in the manufacturer's literature. Several points, however, are of interest. First, every flexural strength specimen broke from an intrinsic flaw and the fracture surface markings were remarkably similar to those of ceramic test pieces, once the lighting or viewing mode was optimized. The similarity to glasses and ceramics should not be surprising due to the high filler content which increased the elastic modulus and strength well above values for the polymer matrix. Once a critical stress intensity level was achieved at a fracture origin, brittle fracture occurred. All loading curves were linear to fracture. There was sufficient stored elastic energy to generate the classical brittle material fracture patterns such as hackle, fracture mirrors, and crack branches as described in [9,26,27]. The fracture origin of every flexural strength bar was easily found with the stereoptical microscope with transillumination and/or vicinal (low angle grazing) illumination. The precise nature of the flaws could not be identified by optical microscopy, but it served to quickly identify an area for close-up SEM examination.

The dominant flaw type in this study was an aluminum inclusion. Two calcium rich inclusions were also detected.

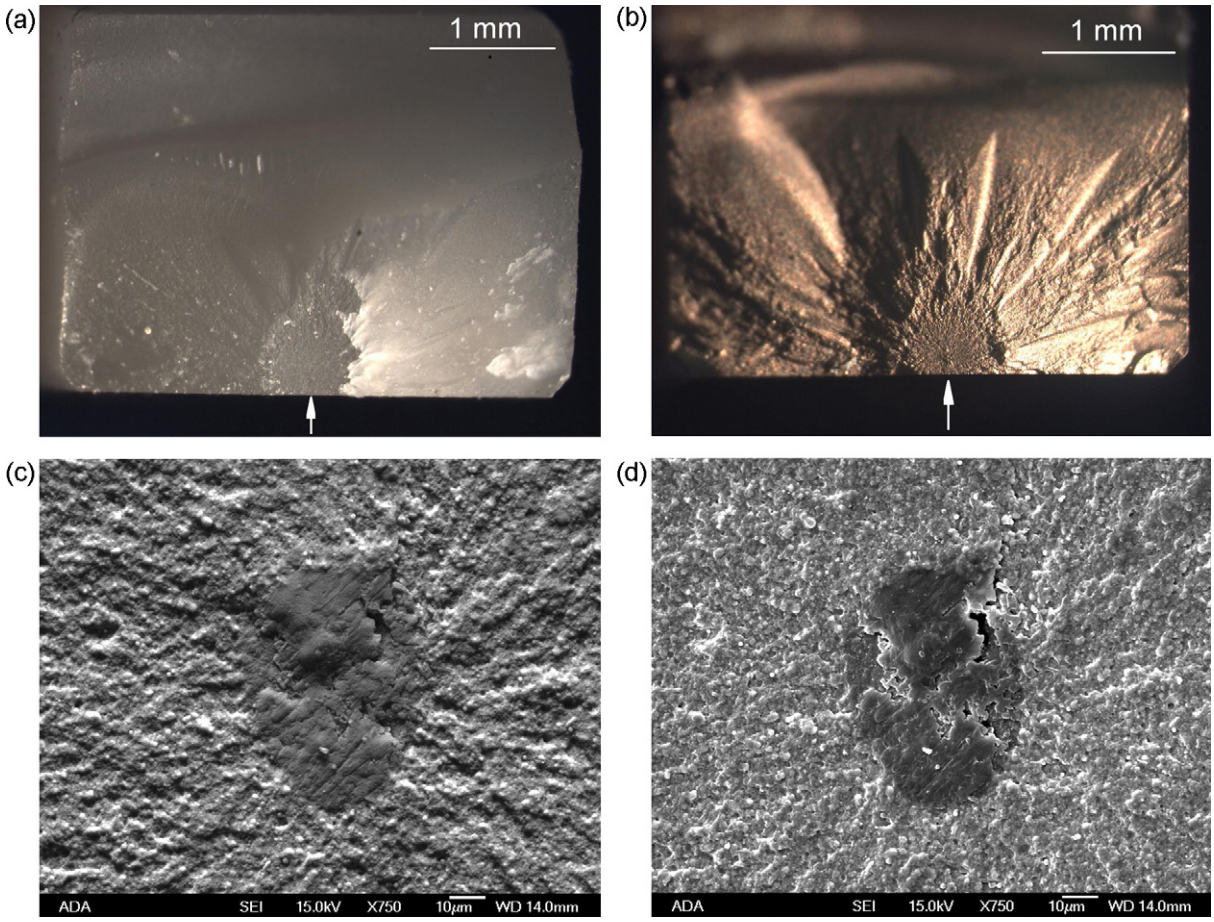

Fig. 6 – Fracture origin in a flexure bar (σ_f = 148 MPa). (a) and (b) are uncoated and gold coated optical images, respectively. The arrows mark the origin. (c) and (d) are backscattered and secondary electron mode SEM images of the calcium rich inclusion flaw, respectively.

Some flaws exhibited traces of chlorine. Two of the fracture origins in the dental composite were volume-distributed spherical flaws that had a chemical composition identical to the matrix. These flaws were probably agglomerates associated with problems in mixing, wetting, or in the distribution of the filler phases in the composite. This is a common outcome for many composite materials, whether they have polymer [1], glass [26], or ceramic matrices [26]. The filler particles in the dental composite were very fine, averaging 0.6 μm. We observed some regions near the origins that were clusters of very fine (<0.2 μm) particles, or debonded regions, or locally porous regions. Some of the flaws may also have had resin rich areas, or regions of incomplete polymerization. Nonuniform distribution of the silane agent commonly used to enhance particle to resin adhesion could also have contributed to some flaws.

Roulin-Moloney [10] identified a number of possible fracture origins in filled resins including air bubbles, resin rich areas, mould lines, foreign matter inadvertently added during moulding, or even the filler particles themselves if they are larger than 100 μm or the particles are inherently weak. Poorly bonded particles can also link up to create a critical flaw that can initiate fracture. Roulin-Moloney [10] showed examples of particle-resin adhesion variability similar to those observed in the present study, albeit with much larger filler particulate sizes.

The variability in the flaw character and size in the dental composite accounts for the modest Weibull modulus (8.0). It should be noted that we did not detect any severe flaws or bubbles in our study and the flaws that were detected were quite small, of the order of 35–100 μm.

The similarity of the calculated K_{Ic} value in this study (1.1 ± 0.2 MPa $m^{1/2}$) based on the flaw size analysis to the company value determined by chevron notch tests (1.3 ± 0.1 MPa $m^{1/2}$, with an unknown number of trials) suggests three possibilities. One possibility is that the fracture toughnesses are the same (within experimental error). Another is that the estimates based on the flaw size analysis may be in error since they were simplistically modeled as sharp cracks, whereas in reality they were three-dimensional flaws. These may have been able to transmit some localized tensile loading across the flaw cross section, unlike a crack. Alternatively, the flaws may have degraded the local fracture toughness. A third possibility is that there is a slightly rising R curve (whereby fracture resistance increases with crack extension) for the material. Shah et al. [32,33] recently reported that rising *R*-curve behavior can occur in similar dental filled resin composites. The slightly greater fracture

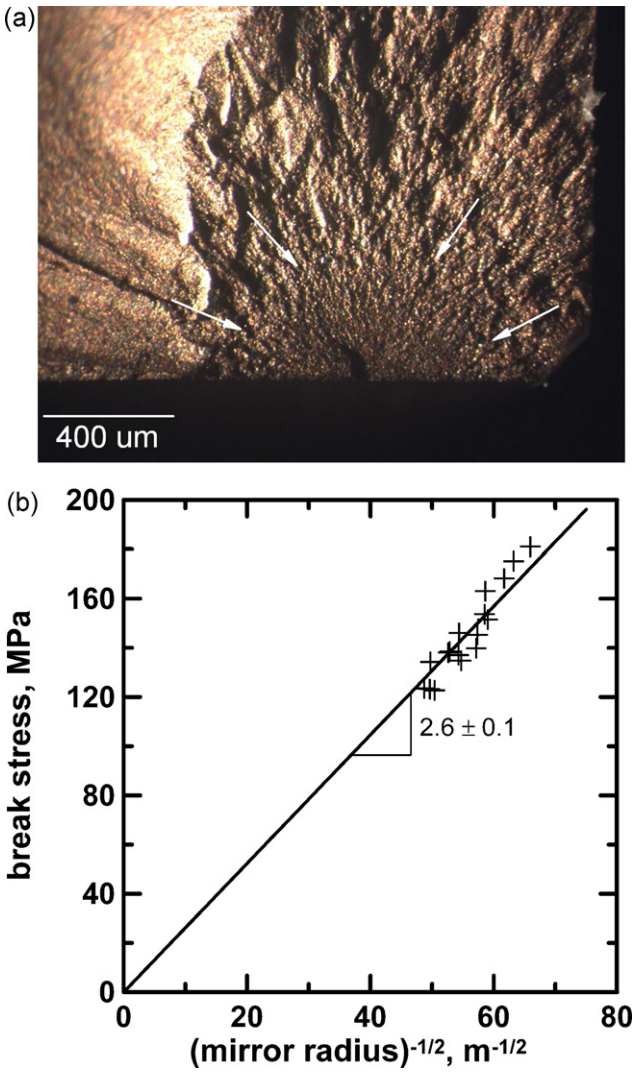

Fig. 7 – Smooth regions surrounding the origin (fracture mirrors) were present in all the specimens: (a) arrows delineate the mirror boundary of the specimen shown in Fig. 3 and (b) graph showing the fracture stress/mirror size relationship. The slope is the mirror constant, A, of 2.6 MPa $m^{1/2}$.

toughness from the chevron notch tests is what one might expect for the larger cracks (of the order of a millimeter) compared to the tens of micrometer-sized intrinsic flaws activated in the strength tests. Shah et al. [32,33] showed the fracture resistance in microhybrid and nanofilled resin composites rose only by about 0.1–0.2 MPa $m^{1/2}$ with crack extensions of the order of 1–3 mm. Fracture toughness values ranged from 0.8 to 1.2 MPa $m^{1/2}$ depending upon the composite system and the amount of crack extension. The filler particles for their microhybrid composite were very similar (and possibly identical) to those in our study. The fracture surfaces in our study showed considerable roughness on the microscopic level with evidence of crack redirection and undercutting along the fracture plane, similar to what Shah et al. [32,33] observed. Future studies could assess whether a rising R-curve exists for this particular material, but our results suggest that it may be inconsequential since the fracture toughness differential is very small. Furthermore, the intrinsic flaws probably become critical before much crack extension has occurred. We could not detect fractographic evidence of local stable crack extension around the critical flaws, but it would appear that the flaws did go critical leading to sudden brittle fracture when they were of the order of tens of micrometers in size. The critical flaw size (radius) was certainly smaller by a factor of five or more than the fracture mirror sizes, the largest of which was about 400 μm in size. As noted above, the R-curves shown by Shah et al. [32] are quite shallow and the full benefit of toughening is not realized until cracks have extended more than 1 mm. In practical terms, it is not likely that clinical restorations with cracks of that size would survive very long to benefit from the meager toughening. So simple estimates of flaw sizes assuming a set value of fracture toughness may be adequate for making approximations in composites with shallow rising R-curves. Nevertheless, Shah et al. [32] did show meaningfully different values of fracture resistance and strength between the two filled composites in their study. Finally, the SCF method probably will not be suitable for other resin composites since precracks do not form underneath the indentation.

A practical consideration is that in vivo resin composite clinical restorations are expected to have the same strengths as the in vitro test specimens if they fracture from similar causes. Accordingly, for indirect restorations of this material type, before installation it might be prudent to examine stress bearing areas for such discontinuities using transillumination. However, if clinical restorations of this material fracture from different causes, such as tool marks, large pores or contact stresses, then the in vitro strength tests would not be a practical predictor of clinical performance, particularly longevity, but only supply an estimated upper limit.

Fracture mirrors were easily detected in this material, which is not surprising in view of its brittle behavior, but their size measurement was more problematic. Although simple in concept and easy to detect, the judgment of a mirror "boundary" to measure can be difficult. Guidelines [26,27] and even a formal standard for ceramics and glasses ASTM C1678 [34] have been adopted, but it is not known whether these procedures are appropriate for resin composites. There is a paucity of data for mirror size constants in such materials. Roulin-Moloney [10] lists only values of 0.82–1.04 MPa $m^{1/2}$ for an unfilled epoxy resin. Nevertheless, our measured value of 2.6 MPa $m^{1/2}$ is 2.4 times the value of the fracture toughness, similar to the relationship observed for some ceramics and glasses. Future work could investigate whether a set of mirror measurement criteria could be established, similar to those for ceramics and glasses.

The load dependence of the hardness tests has particular significance in material comparisons and wear evaluations. A different material is likely to have a different load dependence, and it is difficult to characterize relative hardness without data for the entire force range of importance. If nano-indentations are used to characterize hardness, it can be seen from Fig. 1b that a very small load results in both a higher hardness and a higher variability in measurement. The uncertainty can result from greater difficulties in measuring small indentation sizes, the large change of hardness with small deviations

in force, and most importantly for composite materials, deviations within the microstructure itself. Small indentation areas are more sensitive to the distribution of particles in the resin matrix. Ideally, the indentation area should be large enough to contain a representative distribution of filler particles. The mean size measurement of the 0.25 N indentations in Fig. 1b is only 0.051 ± 0.003 mm. Although the Knoop hardness measurements taken under distilled water were not significantly different from those taken under room conditions, this does not mean that the resin composite hardness is not eventually affected by water. Studies have shown that hardness reduction does occur in resin composites stored in water [35,36]. The current study merely shows that the short-term environmental test conditions have little effect on the measurements.

The edge chipping test was easy to perform, utilized only small amounts of material and edge chipping is a clinically relevant failure mode in resin composites [11,37]. The test results are complicated by a nonlinear relationship, or a line that does not pass through zero. Such a line has no physical meaning, as chips obviously do not form at zero force. A likely explanation for the nonlinearity is material densification before fracture, for similar nonlinear edge-chipping relationships are found for dental glasses, which also densify under force [23]. Densification may possibly play a role in the indentation size effect of the hardness results, as well. A recent model has been developed that does suggest a power law dependence, but with a fixed exponent of 1.5 [38]. Ref. [23] also lists edge toughness values and power law fitting parameters (with exponents ranging from 1.3 to 1.6) for other dental materials. The calculated T_e of the resin composite of 172 N/mm falls about halfway between feldspathic porcelain and glass-infused alumina.

To the best of our knowledge, the fracture origins, fracture mirror and branching constants presented in this work are some of the first such findings for an indirect composite material. The null hypothesis that fractographic analysis can be applied to indirect filled composite is accepted.

5. Conclusions

Fractography can be performed on resin composites, with fruitful results, as an aid in characterizing the material and determining the fracture origins of flexure bars. Transillumination and vicinal illumination are effective with a stereoptical microscope, but the SEM is needed to characterize the nature of the fracture origins. Fractographic techniques may be helpful in determining the strength limiting features of resin composite clinical restorations as well. Also promising is the edge chipping test, which quantifies a material's resistance to a failure mode that is clinically relevant. Finally, hardness was found to be very load-dependent and comparisons of resin composites should be made over a clinically relevant load range, rather than at a single load.

Acknowledgements

The authors appreciate the support of the American Dental Association Foundation, NIST, and NIH Grant R01-DE17983, which made this work possible. We thank 3M-ESPE for furnishing the materials evaluated in this study and appreciate technical discussions with Dr. Richard Rusin.

REFERENCES

[1] Roeters JJM, Shortall ACC, Opdam NJM. Can a single composite resin serve all purposes? Brit Dent J 2005;199:73–9.
[2] Ferracane JL. Current trends in dental composites. Crit Rev Oral Biol Med 1995;6(4):302–18.
[3] Kelly JR. Approaching clinical relevance in failure testing of restorations. J Prosthet Dent 1999;81:652–61.
[4] Quinn GD, Morrell R. Design data for engineering ceramics: A review of the flexure test. J Am Ceram Soc 1991;74(9):2039–65.
[5] Lewis III D. Observations on the strength of a commercial glass-ceramic. Am Ceram Soc Bull 1982;61(11):1208–14.
[6] Taylor D. Strength-component size relationship for high-tension insulator whiteware. Br Ceram Trans J 1989;88:209–12.
[7] Lewis III D, Oyler SM. An experimental test of Weibull scaling theory. J Am Ceram Soc 1976;59(11–12):507–10.
[8] Parrington RJ. Fractography of metals and plastics. Pract Failure Anal 2002;2, 16–19, 44–46.
[9] Rice RW. Ceramic fracture features, observations, mechanisms, and uses. in Mecholsky JJ, Jr., Powell SR, Jr., eds., Fractography of ceramic and metal failures. ASTM STP 827; 1984: p. 5–103.
[10] Roulin-Moloney AC. Fractography and failure mechanisms of polymers and composites. London/New York: Elsevier; 1989.
[11] Lambrecht P, Ameye C, Vanherle G. Conventional and microfilled composite resins. Part II. Chip fractures. J Prosthet Dent 1982;489(5):527–38.
[12] Rusin RP. Properties and applications of a new composite block for CAD/CAM. Compendium 2001;22(Suppl. 6):35–41.
[13] 3M Paradigm, MZ100 Block for CEREC, technical product profile, 3M Center, St Paul, MN; 2000.
[14] ASTM C1161-02. Standard test method for flexural strength of advanced ceramics at ambient temperature. in Annual Book of Standards Vol. 15.01, ASTM, West Conshohocken, PA; 2002.
[15] Baratta FI, Quinn GD, Matthews WT. Errors associated with flexure testing of brittle materials, U.S. Army Materials Technology Laboratory Technical Report, TR 87-35, July; 1987.
[16] ASTM C 1239-06A. Standard practice for reporting uniaxial strength data and estimating Weibull distribution parameters for advanced ceramics; 2006.
[17] Quinn JB, Quinn GD. Indentation brittleness of ceramics: a fresh approach. J Mater Sci 1997;32:4331–46.
[18] McCormick NJ, Almond EA. Edge flaking of brittle materials. J Hard Mater 1990;1(1):25–51.
[19] Watts DC, Issa M, Ibrahim A, Wakiaga J, Al-Samadani, Al-Azraqi M, et al. Edge strength of resin-composite margins. Dent Mater 2008;24(1):129–33.
[20] Baroudi K, Silikas N, Watts DC. Edge-strength of flowable resin-composites. J Dent 2008;36(1):63–8.
[21] Morrell R, Gant AJ. Edge chipping of hard materials. Int J Refract Met Hard Mater 2001;19:293–301.
[22] Gogotsi GA, Mudrik SP. Fracture barrier estimation by the edge fracture test method. Ceram Int 2009;35:1871–5.
[23] Quinn JB, Su L, Flanders L, Lloyd I. Edge toughness" and material properties related to the machining of dental ceramics. Mach Sci and Tech 2000;4:291–304.
[24] Quinn JB, Sundar V, Parry EE, Quinn GD. Comparison of edge chip resistance of PFM and veneered zirconia specimens. Dent Mater 2010;26:13–20.

[25] Quinn JB, Vaderhobli RM. Geometry of edge chips formed at different angles. Ceram Eng Sci Proc 2005;26(2):85–92.
[26] Quinn GD. Guide to practice for fractography of ceramics and glasses, NIST Special Publication SP 960-16, May; 2007.
[27] Quinn GD. Guidelines for measuring fracture mirrors. In: Varner JR, Quinn GD, Wightman M, editors. Fractography of glasses and ceramics, vol. 5. Westerville, OH: American Ceramic Society; 2007. p. 163–90.
[28] ASTM C 1421-99. Standard test method for the determination of fracture toughness of advanced ceramics. Annual Book of ASTM Standards, Vol. 15.01. ASTM, West Conshohocken, PA; 1999.
[29] Scherrer SS, Kelly JR, Quinn GD, Xu K. Fracture toughness of a dental porcelain determined by fractographic analysis. Dent Mater 1999;15(5):342–8.
[30] Newman JC, Raju IS. Stress intensity factor equations for cracks in three-dimensional finite bodies subjected to tension and bending loads. In: NASA Technical Memorandum 85793, NASA Langley Res. Ctr. 1984.
[31] Anderson TL. Fracture mechanics, fundamentals and applications. 2nd ed. New York: CRC Press; 1995.
[32] Shah MB, Ferracane JL, Kruzic JJ. R-curve behavior and micromechanisms of fracture in resin based dental restorative composites. J Mech Behav Biomed Mater 2009;2(5):502–11.
[33] Shah MB, Ferracane JL, Kruzic JJ. R-curve behavior and toughening mechanisms of resin-based dental composites: effects of hydration and post-cure heat treatment. Dent Mater 2009;25(6):760–70.
[34] ASTM C 1678. Standard practice for fractographic analysis of fracture mirror sizes in ceramics and glasses. Annual Book of Standards Vol. 15.01, ASTM, West Conshohocken, PA; 2007.
[35] Da Fonte Porto Carreiro A, Dos Santos Cruz CA, Vergani CE. Hardness and compressive strength of indirect composite resins: effects of immersion in distilled water. J Oral Rehab 2004;31(11):1085–9.
[36] Ferracane JL, Berge HX, Condon JR. In vitro aging of dental composites in water—effect of degree of conversion, filler volume, and filler/matrix coupling. J Biomed Mater Res 1998;42(3):465–72.
[37] Tsitrou EA, Northeast SE, Van Noort R. Brittleness index of machinable dental materials and its relation to the marginal chipping factor. J Dent 2007;35(12):897–902.
[38] Chai H, Lawn BR. A universal relation for edge chipping from sharp contacts in brittle materials: a simple means of toughness evaluation. Acta Mater 2007;55:2555–61.